Supporting information

Adaptable Piezoelectric Hemispherical Composite Strips using Scalable Groove Technique for Self-powered Muscle Monitoring System

Nagamalleswara Rao Alluri[†], Venkateswaran Vivekananthan[$], Arunkumar Chandrasekhar[$], Sang-Jae Kim[$*]

Mailing Address:

[†]**Nagamalleswara Rao Alluri,**

School of Applied Energy Systems (Major in Mechanical Engineering),

Engineering Building No:-4, D-130,

Jeju National University, Ara-1-Dong, Jeju-Si, Jeju-Do

Jeju-690756, South Korea.

Email Id: alluri@jejunu.ac.kr,

[$] **Venkateswaran Vivekananthan, Arunkumar Chandrasekhar,** [*]**Prof. Sang-Jae Kim**

Nanomaterials & System Lab, Department of Mechatronics Engineering,

Engineering Building No:-4, D-130,

Jeju National University, Ara-1-Dong, Jeju-Si, Jeju-Do

Jeju-690756, South Korea.

Email Id: vivek@jejunu.ac.kr, arunecebe@jejunu.ac.kr, kimsangj@jejunu.ac.kr

*Corresponding author (**Prof. Sang-Jae Kim**)

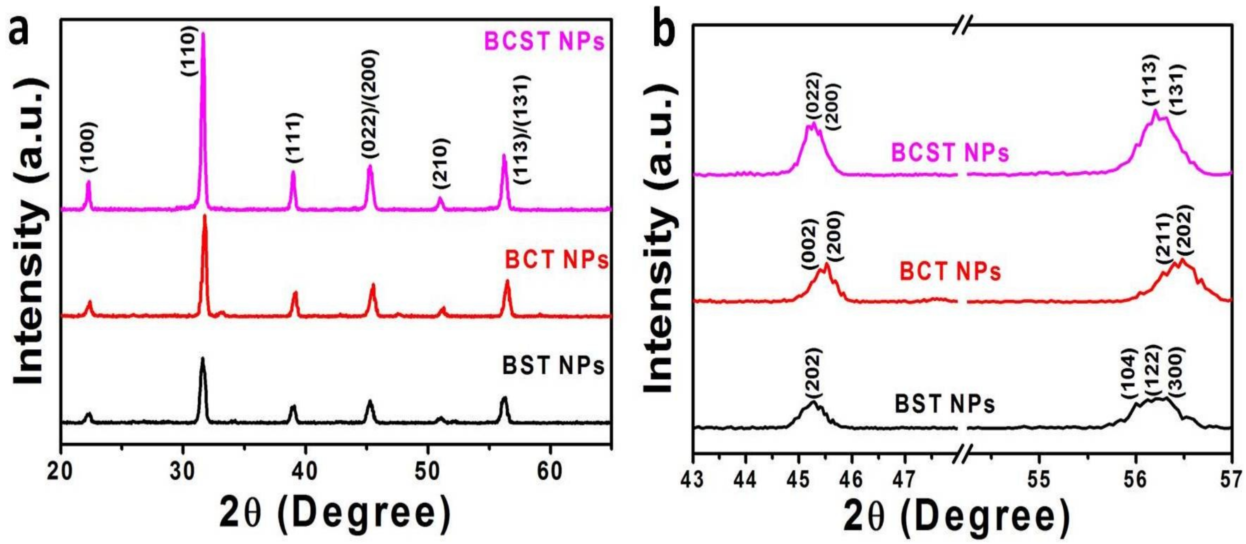

Figure S1 (a) XRD patterns of as-prepared BST, BCT, and BCST NPs prepared *via* high-temperature solid-state reaction. **(b)** A magnified portion (43° to 57°) of XRD patterns for BST BCT and BCST NPs.

High-quality nanocrystalline particles such as BST, BCT and 0.3BCT-0.7BST nanoparticles (designated as BCST NPs) were synthesized using the high temperature (1300 °C/2 h) solid state reaction method. Figure S1 shows the XRD patterns of as-prepared NPs and the corresponding presence of multiple phases, tetragonal (T), orthorhombic (O), and rhombohedral (R), was confirmed by the splitting of peaks at 45–46° and 56°. Here, BCT NPs pattern confirms that the intensity of the $(200)_T$ peak was greater than that of the $(002)_T$ peak, which confirms the T-phase (matched with PDF#05-0626). BST NPs pattern confirms that the $(200)_T$ and $(002)_T$ peaks merged into a broad peak $(202)_R$, which determines the existence of the R-phase (matched with PDF#85-0368). These phase variations attributed to the substitution of foreign atoms having different ionic radii, i.e., Sn^{4+} (0.69 Å) and Ca^{2+} (1.34 Å), into Ti^{4+} (0.605 Å) and Ba^{2+} (1.61 Å) atomic sites of the $BaTiO_3$ (BTO) lattice, which created internal lattice strains in various directions. The dual system BCST NPs pattern confirms the existence of multiple phases, i.e., the splitting of peaks at 45–46° and 56°, which is well matched with the reference pattern ID = PDF#81-2200.

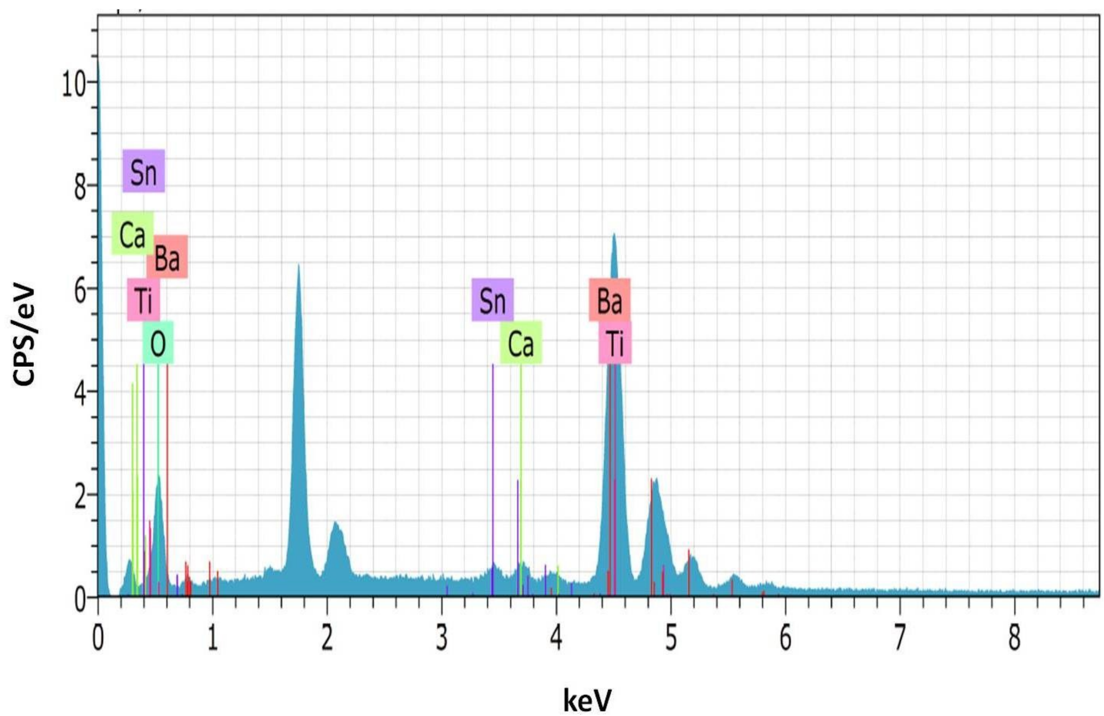

Figure S2 Elemental characterization of BCST NPs using the energy dispersive X-ray spectroscopy.

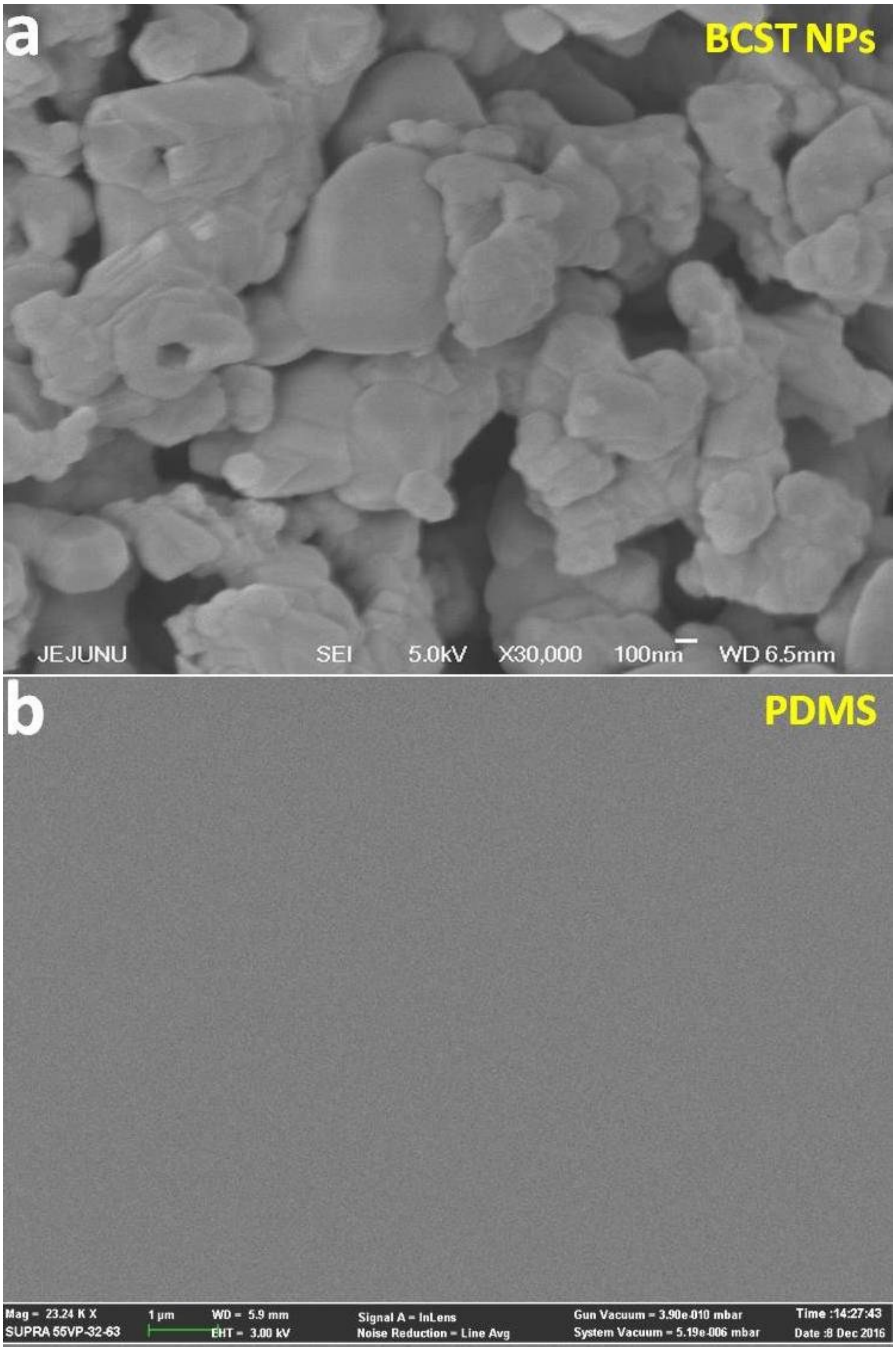

Figure S3(a) Highly random oriented nanocrystalline surface morphology of BCST NPS. **(b)** FE-SEM image of pure PDMS matrix confirms the smooth surface morphology.

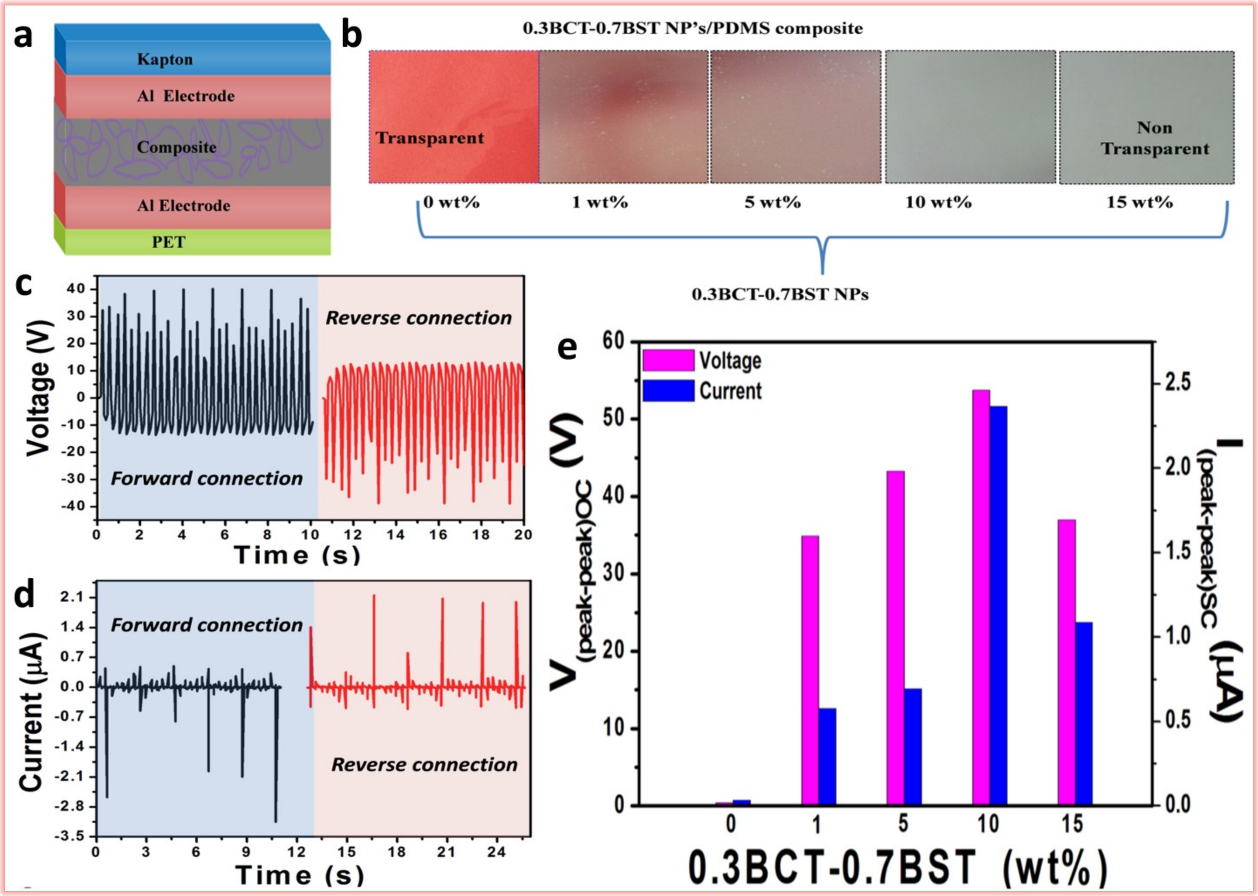

Figure S4 Planar P-NG electrical response upon constant mechanical force 30 N. **(a)** Device schematic diagram **(b)** As-prepared BCST NPs/PDMS composite films and its transparency behavior. **(c, d)** Switching polarity test and electrical response analysis of P-NG (10 wt% of BCST NPs/PDMS) **(e)** cumulative peak-to-peak electrical response of all P-NGs with various wt% of BCST NPs, upon constant mechanical force 30 N.

Initially, we performed the planar P-NG (area ≈3 × 2.5 cm^2) electrical response analysis using BCST NPs/PDMS matrix composite film along with the various weight ratios of BCST NPs (0, 1, 5, 10, and 15 wt%). All these planar P-NGs (Polyethylene terephthalate (PET)/Aluminium (Al)/Composite film/Al/Kapton) performance tested with the constant mechanical force. Figure S4a shows the basic planar P-NG schematic diagram. The transparency of PDMS decreased with increasing the weight fraction of 0.3BCT-0.7BST NPs as shown in Figure S4b. The open circuit voltage (≈55 V) and short-circuit current (≈2.23 μA) response of the P-NG device (10 wt %) upon constant force 30 N shown in Figure S4 (c, d). The switching polarity test (forward/reverse connections) of P-NG device confirms that the generated electrical output response is a true response, not coming from any other external sources. Similar electrical responses analyzed for all weight ratios of NPs based P-NG devices, and the corresponding peak-to-peak electrical response shown in Figure S4e. The electrical output increased with increasing weight fraction of NPs (up to 10 wt %), but the electrical output steadily decreased beyond 10 wt%. The decrement of the electrical output of P-NG, greater than 10 wt% is due to maybe two factors such as relative change of piezoelectric coefficient (d_{33}) is lower than the relative change of the effective dielectric constant (ε_{eff}) and second is an agglomeration of BCST NPs. A higher weight fraction of the piezoelectric NPs in the PDMS matrix could lead to agglomeration, in which case the applied force on the P-NG device maybe not distributed uniformly over all of the NPs. This leads to a non-uniform orientation of the electric dipoles, and some of the electric dipole moments in the film could cancel each other. This mechanism would account for the low electrical output for the composite P-NG device prepared with greater than 10 wt% of NPs. Moreover, this planar P-NG device not suitable to monitor all human body part movements.

The above analysis demonstrates that 10 wt% of BCST NPs in PDMS matrix is highly suitable for better energy conversion. Because of this reason, we selected 10 wt% of BCST NPs in PDMS for developing the highly adaptable, flexible hemispherical piezoelectric composite strips. These strips highly suitable to monitor maximum human body part movements.